Available online at www.sciencedirect.com
SCIENCE DIRECT®
Journal of Molecular Graphics and Modelling 24 (2006) 440–455
Journal of Molecular Graphics and Modelling
www.elsevier.com/locate/JMGM

Quantum mechanical description of the interactions between DNA and water

Lance M. Westerhoff, Kenneth M. Merz Jr.*

Department of Chemistry, 104 Chemistry Building, The Pennsylvania State University, University Park, PA 16802, USA

Received 14 July 2005; received in revised form 24 August 2005; accepted 26 August 2005
Available online 30 September 2005

Abstract

In recent years, a lot of attention has been focused on the electronic properties of DNA. With recent advances in linear scaling quantum mechanics there are now new tools available to enhance our understanding of the electronic properties of DNA among other biomolecules. Using both explicit solvent models and implicit (continuum) solvent models, the electronic characteristics of a dodecamer duplex DNA have been fully studied using both divide and conquer (D&C), semi-empirical quantum mechanics and non-D&C semi-empirical quantum mechanics. According to the AM1 Hamiltonian, ~3.5 electrons (~0.3 electron/base pair) are transferred from the duplex to the solvent. According to the density of state (DOS) analysis, in vacuo DNA has a band gap of ~1 eV showing that in the absence of solvent, the DNA may exhibit similar properties to those of a semiconductor. Upon increasing solvation (2.5–5.5 Å), the band gap ranges from ~3 eV to ~6 eV. For the implicit solvent model, the band gap continues this widening trend to ~7 eV. Therefore, upon solvation and in the absence of dopants, the DNA should begin to loose its conductive properties. Finally, when one considers the energy and localization of the frontier orbitals (HOMO and LUMO), solvent has a stabilizing effect on the DNA system. The energy of the HOMO drops from ~15 eV in vacuo to ~2 eV for 5.5 Å of water to ~−8 eV for the implicit solvent model. Similarly, the LUMO drops from ~16 eV for in vacuo to ~9 eV for 5.5 Å of water to ~−1 eV for the implicit model. Beyond the importance of the computed results on the materials properties of DNA, the present work also shows that the behavior of intercalators will be affected by the electronic properties of DNA. This could have an impact on our understanding of how DNA based drugs interact with DNA and on the design of new DNA based small molecule drugs.

Keywords: Quantum mechanics; DNA; Water; Frontier orbital distribution; Density of state analysis; Highest occupied molecular orbital; HOMO; Lowest unoccupied molecular orbital; LUMO; Explicit solvation; Continuum solavation

1. Introduction

Through the use of molecular dynamics, semi-empirical quantum mechanics, and molecular modeling, the data presented in this paper furthers our understanding of the charge dynamics, the frontier orbital characteristics, and the conductive properties of solvated and unsolvated (in vacuo) deoxyribonucleic acid (DNA) systems. Further, an understanding of the electrical processes of DNA could lead to a better appreciation of both the mechanisms of DNA damage and of DNA repair [1].

Structurally, a standard DNA double helix consists of two strands of four possible bases (Fig. 1): adenine, guanine, cytosine, and thymine. Analogous to rungs on a ladder, each base of one strand is hydrogen bonded to a complementary base on the opposite strand where every guanine on the first strand is paired to a cytosine on the second strand through three hydrogen bonds, and each adenine on the first strand is paired with a thymine on the second strand through two hydrogen bonds. Attached to each base is the sugar ribose (Fig. 1) and the ribose is attached to its neighbors with a phosphate group (Fig. 2). Each phosphate group contains a single negative charge and, as depicted in Fig. 3, this phosphate group is accessible to solvent [2].

It is well documented that water plays a crucial role in the stabilization of biomolecular systems [3] and that much of this is due to the hydrogen bonding capability of water [4]. This stabilization is generally explained using classical bonding models where the electrostatic nature of the hydrogen bonds can be simulated [5,6]. The forces associated with these interactions are, therefore, usually modeled successfully using a combination of Coulomb and Lennard–Jones interactions. Recently, extensions beyond this simple classical pair potential

* Corresponding author. Tel.: +1 814 865 3623; fax: +1 814 865 3292.
E-mail address: merz@psu.edu (K.M. Merz Jr.).

1093-3263/$ – see front matter © 2005 Elsevier Inc. All rights reserved.
doi:10.1016/j.jmgm.2005.08.010

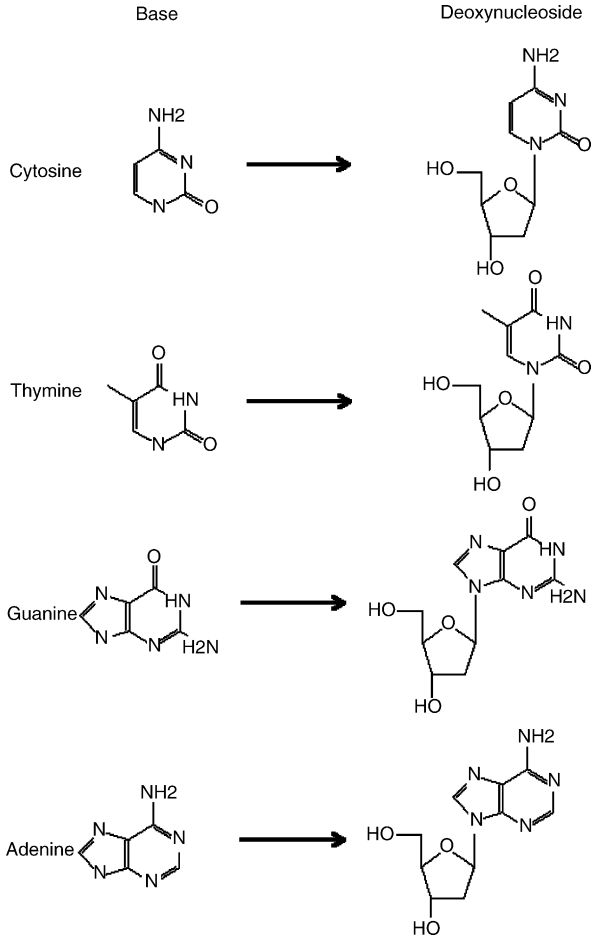

Fig. 1. Chemical structures of each of the DNA nucleosides. DNA consists of four possible bases. Each of these bases is bound to a deoxyribose molecule to form a nucleoside.

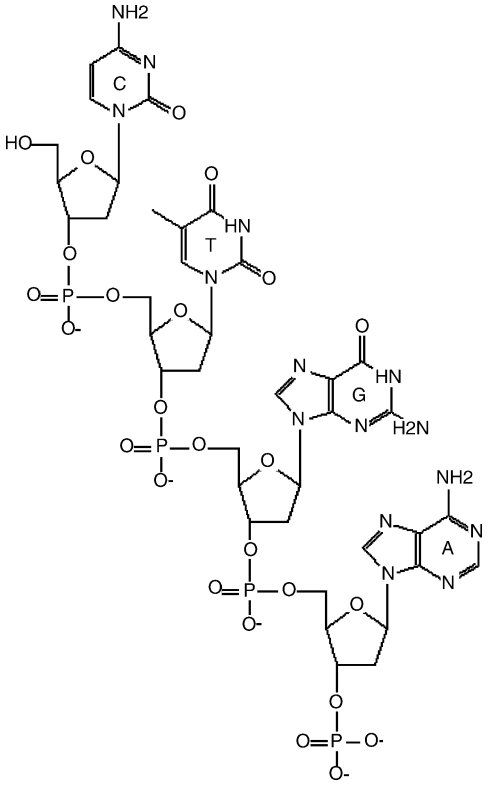

Fig. 2. Formation of the DNA backbone. In DNA, each of nucleosides is with a negatively charged phosphate group to form a nucleotide. These nucleotides are then joined together to form the DNA backbone.

have been implemented which include polarization to more accurately represent intramolecular electronic reorganization indicative of interactions between two or more molecules [7,8]. This polarization is shown to contribute approximately 10% of the total intramolecular interaction energy [9]. However, recent research by van der Vaart and Merz [5,6] has provided evidence that in biomolecular systems the intramolecular interaction energy due to charge transfer (intermolecular charge rearrangement) is significant. Since DNA carries a highly negative, solvent accessible charge, studies on systems with DNA should provide further insights into the differing effects of charge transfer, polarization, and electrostatics in solvent–solute interactions.

Another interesting topic is oxidative stress or damage to DNA. In order for DNA to replicate, the two strands will separate exposing the non-hydrogen bonded bases to solvent. Once the stands are separated, another set of proteins passes along each strand in order to replicate the previously bonded stand by successfully hydrogen bonding complementary bases to the original strand. When this process is completed and if the process was successful, two identical double helices should exist where once there was one [10]. If a base is oxidized, there are several possible structural problems that can occur causing future replication or transcription to fail leading to deleterious conditions which may include mutations, cancer, or even aging [11–14]. These problems can include single point mutations due to the identity of a single base being masked with the loss of a hydrogen bond [2], strand breakage [2,15,16], thymine dimmers [1] or pyrimidine dimmers [17], and in the case of aging, build up of missense mitochondrial DNA (mtDNA) [14]. Interestingly, in addition to these negative effects, oxidative stress has been attributed to certain mechanisms of DNA repair [1].

Of particular interest and debate, are the effects of long-range DNA damage when electron transfers are observed over longer distances [18]. Long-range charge transfer has been observed in single DNA molecules [19], in ropes consisting of a few DNA molecules [20], in thin films of DNA molecules [21], in DNA in aqueous glasses [22], in crystalline DNA [23], in intercalated solvated DNA [24–40] and in solvated DNA with modified bases. The idea of long-range electron transfers or conductance is still a matter of debate in DNA, but much of the experimental [35,41] and theoretical [16] evidence seems to support that it does indeed occur. Three major mechanisms have been proposed leading to continued debate on the subject.

The first of these mechanisms is that DNA can act as a ‘‘molecular wire’’ where the π-stack of the hydrogen bonded base pairs of the double helix acts as a conduit for charge. Although this model would require a low activation energy to facilitate charge flow, it requires strong electronic coupling between the donor and the acceptor species [30,40]. In a second proposed mechanism, DNA would exhibit qualities similar to a

(a)

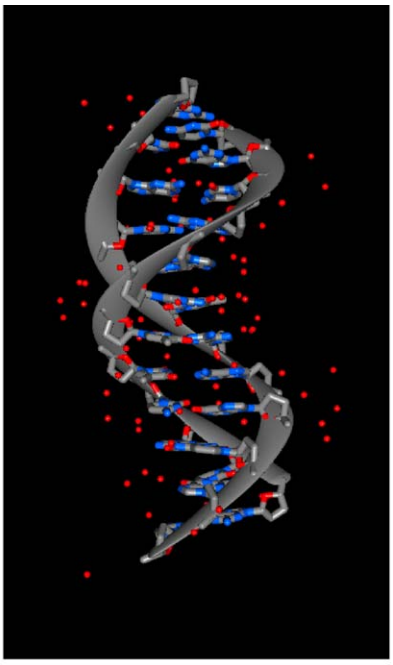

(b)

```
346-379 G3  (12) === (13) C5  380-407
316-345 C   (11) === (14) G   408-440
283-315 G   (10) === (15) C   441-470
253-282 C   (09) === (16) G   471-503
221-252 T   (08) === (17) A   504-535
189-220 T   (07) === (18) A   536-567
157-188 A   (06) === (19) T   568-599
125-156 A   (05) === (20) T   600-631
092-124 G   (04) === (21) C   632-661
062-091 C   (03) === (22) G   662-694
029-061 G   (02) === (23) C   695-724
001-028 C5  (01) === (24) G3  725-758
```

Fig. 3. Model of the Dickerson Dodecamer. (a) The graphical model of the Dickerson Dodecamer (PDB ID: 1BNA). The red spheres signify the crystal waters found within the structure. (b) Illustration of the sequence of the model where the xxx–xxx numbers signify the range of atoms included in the residue number in parenthesis.

semiconductor in that the electron transfer would occur through a molecular band. In this model, the electronic states are delocalized over the entire length of the molecule similar to a semi-conductor, and charge is transferred through the movement of an electron or hole [19]. In the third proposed mechanism, the charge is transferred through a hopping mechanism where the charge would hop between neighboring bases with a required activation energy of approximately 5 kcal/mol. In this model, no coupling between the donor and the acceptor is required, and the charge carrier is in the form of a hole (radical cation) or an electron (radical anion) [39,42–44].

Theoretical studies on the tunneling and the hopping models have been performed on simplified DNA strands in vacuum [45–48]. Due to its immense size, the computational expense required to quantum mechanically characterize this important biomolecule tends to be prohibitively large. Ab initio calculations are generally limited to single hydrogen bonded and stacked base pairs [49–52] while, in the past, semi-empirical calculations were limited to DNA strands embedded in a dielectric continuum [53]. The continuum study shows that the band-gap will disappear in a continuum and appear in a vacuum. However, since explicit water molecules have a significant effect on the electron structure of proteins [54,5,6], it can be assumed that a similar significance should be observed in highly charged DNA systems. Therefore, to properly describe the electronic structure of DNA, inclusion of explicit solvent (water) molecules may be necessary.

Unfortunately, inclusion of explicit water molecules increases the computational expense of the simulation and only in the past several years researchers have witnessed the development of linear scaling methodologies required to quantum mechanically solve these large systems. The study presented in this paper employs linear scaling, divide and conquer (D&C), semi-empirical quantum mechanics [55–57] for treatment of explicit DNA–water systems and divide and conquer, Possion–Boltzman (DCPB) methods [58] for treatment of systems using a dielectric continuum in place of water. Together, these methods should provide a better understanding of the electronic properties of DNA and the long-range interactions it exhibits. Secondarily, the use of both the explicit water method and the continuum method should provide a basis for a comparison of both methods for biological systems in general.

In addition to the conductive properties of DNA, the results in this study will show evidence concerning the most reactive residues in the molecule. It has long been accepted that interactions between the highest occupied molecular orbital (HOMO) of organic molecules with the lowest unoccupied molecular orbital (LUMO) of organic molecules plays a critical role in chemical reactions of organic molecules [59,60] and larger biomolecules [61,62]. Until recently, the HOMOs and LUMOs of biomolecular systems have remained largely unstudied due to the limitations associated with quantum mechanical methods and the size of the system. Ab initio calculations have been limited to stacked 5′-GG-3′ bases [63,51] and short duplexes of stacked, complementary bases of various sequences [62]. In all cases, the bases lacked a ribose–phosphate backbone and were uncharged. Further, these studies were performed in vacuo and therefore, did not attempt to simulate solvent characteristics either explicitly or implicitly (continuum conditions). Based on previous work with proteins [58,5,6,64,65] showing that both the atomic charge of the system and the solvation environment play pivotal roles in the electronic distribution of the biomolecule, the accuracy of these ab inito data may be suspect. The same linear scaling, semi-empirical quantum mechanics methods noted above which allow computational biochemists to study large biomolecular systems can yield fundamental insights into the energies and the localization of these reactive frontier molecular orbitals (FMOs). The FMO results along with the charge transfer characteristics will give us a deeper understanding to the reactivity of DNA and the localization of those areas most receptive to biomedical targeting [66].

2. Methods

The “Dickerson Dodecamer” [67] served as a starting point for the simulations (see Fig. 3). The three dimensional structure

Table 1
Summaries for the each of the 25 configurations[a]

	0.0 Å			2.5 Å			3.5 Å			4.5 Å			5.5 Å		
	A	B	C	A	B	C	A	B	C	A	B	C	A	B	C
100	758	0	−22	1502	248	−22	1977	406	−21	2508	582	−18	3032	756	−16
200	758	0	−22	1488	243	−21	1967	402	−19	2509	582	−17	3063	766	−15
300	758	0	−22	1488	243	−21	1939	393	−20	2513	583	−16	3008	747	−13
400	758	0	−22	1506	249	−21	1925	388	−19	2484	573	−15	3047	760	−13
500	758	0	−22	1532	258	−22	1892	377	−19	2477	571	−16	2960	731	−13

[a] The A columns refer to the total number of atoms. The B columns denote the number of water molecules in the configuration while the C columns refer to the total charge on the system. The number of sodium atoms is 22 (the absolute in vacuo DNA charge) minus the absolute charge of the configuration.

of this molecule has been solved to 1.9 Å using X-ray crystallography and has been well studied since its structure was solved in 1981. Although its sequence, 5′-CGCGAATTCGC-3′ (Fig. 3b), does not include guanine doublets or triplets as studied by other groups [51,41,62], it does include two separate stretches of G–C pairs which have also been shown to exhibit reactivity [62]. In the future, further studies could be performed which will more closely match sequences of special interest to other laboratories.

The Dodecamer, along with its associated ‘‘crystal waters’’ (red oxygen spheres shown in Fig. 3a) was placed in a rectangular box of 4453 TIP3P [68] waters as configured using the Link/Edit/Parm programs included in the AMBER5.0 [69] package. The phosphate groups of the Dodecamer endowed the double helix with an overall molecular charge of −22. Generally, molecular dynamics simulations incorporating DNA require the inclusion of positively charged counterions in the simulation in order to maintain the hydrogen bonds securing the two strands of DNA together [70]. Therefore, in order to offset the −22 charge and maintain duplex stability, 22 Na^+ (sodium) ions were also included in the simulation box.

Once the duplex was solvated and a overall zero charge was placed upon the simulation box, the DNA–water system was minimized with 200 steps of steepest decent followed by 9800 steps with the conjugate gradient minimizer as implemented in the ROAR1.1 [71] program included in the AMBER5.0 package using the AMBER force field [72]. The Sander5.0 module of the AMBER5.0 package was used to perform the actual molecular dynamics simulation by initially subjecting the system to a 27 ps MD equilibration followed by a 500 ps MD simulation. In both the equilibration and the simulation, a time step of 0.015 ps was employed, and the temperature and pressure of the system were maintained at 300 K and 1 bar, respectively, using the Berendsen et al. [73] algorithm. In order to further mimic natural, biological conditions, periodic boundary conditions were in effect, and Ewald [74] summation was employed to handle long-range interactions.

Upon completion of the MD simulation, five conformation snapshots were derived at 100 ps, 200 ps, 300 ps, 400 ps, and 500 ps. Each of these snapshots was further manipulated to include solvent within 0.0 Å, 2.5 Å, 3.5 Å, 4.5 Å, and 5.5 Å away from the DNA. Together, the vacuum structure and the systems of varying solvation shell width consisted of five configurations for each of the five sampled snapshots to finally yield a grand total of 25 different configurations (see Table 1). Since the configurations included any Na^+ counterions that fell within the respective solvation shells, the overall charge of each of the configurations varied between from −22 for vacuum to −13 for some of the more highly solvated systems.

Quantum mechanical calculations using both the AM1 Hamiltonian [75] and the PM3 Hamiltonian [76,77] were performed on each of the 25 configurations using the DivCon99 program [78]. Since artificial leakage of states into the HOMO–LUMO gap has been observed when employing the linear scaling, divide and conquer method [55–57], the much more computationally expensive ‘‘standard’’ or non-D&C method was employed in the final steps of the study. In order to facilitate SCF convergence in these systems, the D&C method was initially used to generate increasingly improved density matrices to serve as guesses for the standard calculations. A cut-off of 8 Å for the one-electron, Fock, and density matrices was used in all of the semi-empirical calculations presented in this work. After the standard calculations were complete, a full DNA–solvent interaction energy decomposition [5,6] was performed. In all cases, the parameters for the Na^+ ions included in the explicit solvent configurations were those of Brothers and Merz [79].

In addition to these explicit solvent models, implicit solvent or continuum calculations were also performed using the Possion–Boltzman continuum method [58] available in DivCon99. These calculations were performed on each of the five (in vacuo) snapshots employing both Hamiltonians. Again, the final step of these calculations used a standard, non-D&C continuum approach, and in each case a guess, in vacuo density matrix generated using the D&C approach on each 0.0 Å configuration, was provided as a starting point for the calculations.

3. Results and discussion

3.1. Charge dynamics

Previous research has shown that solvation is important in biomolecular charge stabilization through various solvent-solute interactions [5,6,64,65]. The highly charged DNA studied in our research is no different, and the inclusion of explicit water is shown to be crucial to fully understand the charge distribution of DNA. For the sake of completeness, the results of both the AM1 Hamiltonian and the PM3 Hamiltonian are provided in this paper, but a more significant weight should

Table 2
AM1 charge transfer at the DNA–water interface[a]

	2.5 Å	3.5 Å	4.5 Å	5.5 Å	Average	S.D.
100 ps	3.3747	3.4616	3.4928	3.4770	3.4515	0.0528
200 ps	3.4267	3.4537	3.4979	3.4680	3.4616	0.0297
300 ps	3.5687	3.5410	3.5456	3.5032	3.5396	0.0271
400 ps	3.8127	3.8736	3.8587	3.8451	3.8476	0.0260
500 ps	3.2638	3.2980	3.2828	3.2681	3.2782	0.0155
Average	3.4893	3.5256	3.5355	3.5123	3.5157	
S.D.	0.2114	0.2136	0.2072	0.2084		0.1937

[a] There is a slight dependence both on the time step and the level of solvation. The standard deviations of each of the columns is an order of magnitude greater then those of the rows showing that there is a higher dependence on the conformation (time step) then on the level of solvation. Since the standard deviations for the rows are so small, one can assume that the amount of charge transfer converges upon initial solvation and that it is this first solvation layer that is most important.

probably be placed on the AM1 results since AM1 predicts the amount of charge transferred better than PM3 [64,65].

As seen in Table 2 for AM1 and Table 3 for PM3, the negatively charged DNA systems exhibit a flow of ∼3.5 electrons for AM1 and ∼5.3 electrons for PM3 from the DNA to the surrounding solvent. Specifically, the AM1 Hamiltonian shows that on average, per base pair ∼0.3 electron are transferred to the solvent. Similarly, the PM3 Hamiltonian shows an average of ∼0.5 electron per base pair, transferred to the surrounding solvent. Also as shown in Tables 2 and 3, there is no significant increase in charge transfer with increasing levels of solvation signifying that the charge stabilization converges when the level of solvation reaches 2.5 Å. Further analysis reveals that the transferred charge remains localized in the first solvation layer and that the charge is not smeared out beyond this boundary further supporting previous works with protein–water systems [54,5,6].

In addition to these more general trends, we can determine which atomic species exhibit the greatest (and least) influence or charge transfer. A more in depth investigation of the results shows that most of the charge was transferred from the phosphate groups (Tables 4 and 5) where most of the charge is transferred from the phosphate oxygen atoms. Positive CM2 charges signify that the charge is transferred from the group and negative CM2 charges refer to charge being accepted by the atom from its surroundings. As expected from the overall charge transfer shown in Tables 2 and 3, most of the atoms exhibiting significant charge transfer lose charge while only a few gain charge.

Table 3
PM3 charge transfer at the DNA–water interface[a]

	2.5 Å	3.5 Å	4.5 Å	5.5 Å	Average	S.D.
100 ps	5.1166	5.2567	5.3193	5.3098	5.2506	0.0935
200 ps	5.1499	5.2325	5.3214	5.3046	5.2521	0.0783
300 ps	5.3893	5.4153	5.4508	5.4069	5.4156	0.0258
400 ps	5.6255	5.7376	5.7487	5.7542	5.7165	0.0611
500 ps	5.0710	5.1348	5.1412	5.1290	5.1190	0.0324
Average	5.2705	5.3554	5.3963	5.3809	5.3508	
S.D.	0.2336	0.2362	0.2257	0.2315		0.2185

[a] There is a slight dependence both on the time step and the level of solvation. The standard deviations of each of the columns is an order of magnitude greater then those of the rows showing that there is a higher dependence on the conformation (time step) then on the level of solvation. Since the standard deviations for the rows are so small, one can assume that the amount of charge transfer converges upon initial solvation and that it is this first solvation layer that is most important.

Table 4
AM1 data showing charge flow to/from various atoms[a]

Atom	Group	Average	S.D.
OC	Phosphate	0.0454	0.0133
P	Phosphate	0.0200	0.0048
O2	Thymine	0.0051	0.0028
O4	Thymine	0.0070	0.0036
O2	Cytosine	0.0069	0.0053
O6	Guanine	0.0092	0.0051
N3	Adenine	0.0070	0.0056
N7	Adenine	0.0126	0.0074
N3	Guanine	0.0053	0.0046
N7	Guanine	0.0089	0.0050
H3	Deoxyribose	−0.0057	0.0040

[a] Certain key atoms within the DNA system show significant charge flow to and from various atoms. The CM2 charges were used to show the amount of charge transfer where positive numbers indicate that the charge is transferred from the atom and negative values show an increase in negative charge due to charge being transferred into the atom.

3.2. Density of state analysis

The density of state (DOS) analysis provides an understanding of the energy distributions of the frontier molecular orbitals found in a chemical system. Fig. 4 compares the 5.5 Å solvation configuration of each snapshot with the in vacuo configurations for each snapshot. In every case, the greater solvation causes the FMOs to be more stabilized (lower in energy). A more detailed examination is presented

Table 5
PM3 data showing charge flow to/from various atoms[a]

Atom	Group	Average	S.D.
OC	Phosphate	0.0615	0.0146
P	Phosphate	0.0383	0.0050
O3	Deoxyribose	0.0064	0.0064
O5	Deoxyribose	0.0056	0.0058
O2	Thymine	0.0110	0.0050
O4	Thymine	0.0141	0.0059
O2	Cytosine	0.0139	0.0089
O6	Guanine	0.0179	0.0083
N3	Adenine	0.0226	0.0144
N7	Adenine	0.0377	0.0192
N3	Guanine	0.0162	0.0127
N7	Guanine	0.0293	0.0149
N2	Guanine	−0.0066	0.0076
N4	Cytosine	−0.0065	0.0077
H3	Deoxyribose	−0.0051	0.0040

[a] Certain key atoms within the DNA system show significant charge flow to and from various atoms. The CM2 charges were used to show the amount of charge transfer where positive numbers indicate that the charge is transferred from the atom and negative values show an increase in negative charge due to charge being transferred into the atom.

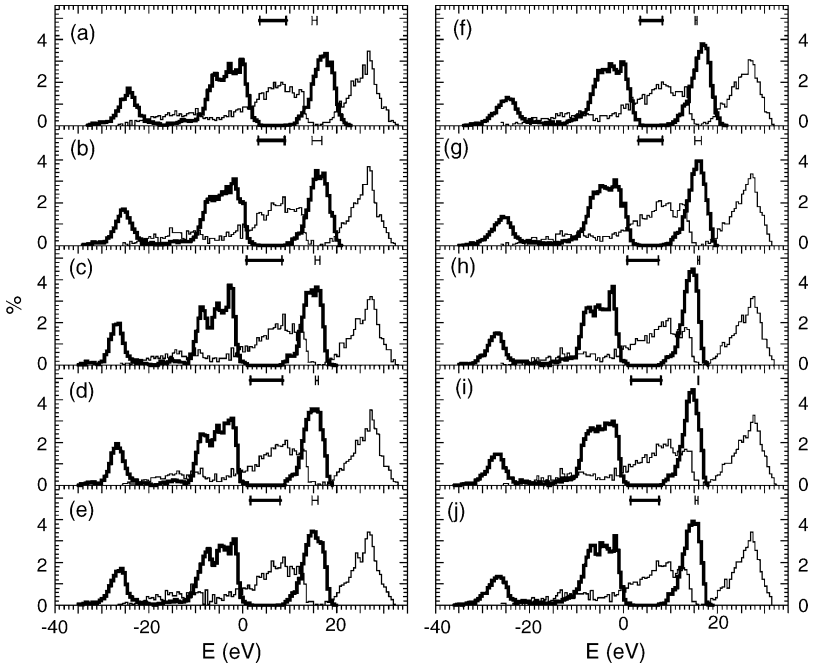

Fig. 4. Density of state of solvated DNA and DNA in vacuum. This figure compares of the results from 5.5 Å solvation layer calculation (in bold) with the results of the DNA in vacuum calculation. The horizontal lines indicate the HOMO–LUMO gap. The figure is broken down both by Hamiltonian and by time step. On the left side (a–e) shows the results of the AM1 Hamiltonian at 100 ps, 200 ps, 300 ps, 400 ps, and 500 ps, respectively. The right side (f–j) shows the results of the PM3 Hamiltonian at 100 ps, 200 ps, 300 ps, 400 ps, and 500 ps, respectively.

in Tables 6 and 7, which show the HOMO energies while Tables 8 and 9 show the changes in LUMO energies with increasing solvation. For both HOMO energies and LUMO energies, the level of solvation causes the energies to shift to lower values. The average HOMO energy shift is as much as 12.8 eV for AM1 and 13.3 eV for PM3 while the LUMO energy shift is only 7.6 eV for AM1 and 8.1 eV for PM3. This disproportionate decrease in energy levels between the HOMOs

Table 6
HOMO energies determined using the AM1 Hamiltonian[a]

	0 Å	2.5 Å	3.5 Å	4.5 Å	5.5 Å	DCPB	Average	S.D.
100 ps	14.7753	12.4522	9.6502	6.0561	3.6062	−8.1878	6.3920	8.2227
200 ps	14.7428	11.5904	8.1886	5.7960	3.3022	−8.1698	5.9084	8.0066
300 ps	15.2971	11.8595	10.0358	4.6267	0.8472	−8.1022	5.7607	8.5326
400 ps	15.3844	11.6786	8.9609	3.5144	1.6410	−8.1092	5.5117	8.3893
500 ps	14.8063	12.7277	8.9761	4.7660	1.6361	−8.1561	5.7927	8.3949
Average	15.0012	12.0617	9.1623	4.9518	2.2065	−8.1450	5.8731	
S.D.	0.3123	0.5015	0.7114	1.0172	1.1888	0.0377		7.7224

[a] The density of state analysis shows the energy, measured in eV, of the highest occupied molecular orbital as a function of simulation time and solvation. One can observe the trend from the 0 Å water layer to DCPB (continuum) water that the HOMO energies become increasingly stabilized as the system becomes increasingly solvated, while at the same time; the conformational dependence is much less distinct.

Table 7
HOMO energies determined using the PM3 Hamiltonian[a]

	0 Å	2.5 Å	3.5 Å	4.5 Å	5.5 Å	DCPB	Average	S.D.
100 ps	15.2474	12.6307	9.7976	6.1452	3.5567	−7.8584	6.5865	8.2448
200 ps	15.1845	11.6949	8.2604	5.7893	3.2446	−7.9054	6.0447	8.0359
300 ps	15.7222	11.9615	10.0606	4.5349	0.8071	−7.8294	5.8761	8.5653
400 ps	15.8280	11.7199	8.9105	3.4344	1.6032	−7.8490	5.6078	8.4210
500 ps	15.2726	12.8458	9.0246	4.6925	1.5865	−7.8479	5.9290	8.4252
Average	15.4509	12.1706	9.2107	4.9193	2.1596	−7.8580	6.0088	
S.D.	0.3000	0.5340	0.7236	1.0798	1.1829	0.0285		7.7508

[a] The density of state analysis shows the energy, measured in eV, of the highest occupied molecular orbital as a function of simulation time and solvation. One can observe the trend from the 0 Å water layer to DCPB (continuum) water that the HOMO energies become increasingly stabilized as the system becomes increasingly solvated, while at the same time; the conformational dependence is much less distinct.

Table 8
LUMO energies determined using the AM1 Hamiltonian[a]

	0 Å	2.5 Å	3.5 Å	4.5 Å	5.5 Å	DCPB	Average	S.D.
100 ps	15.8430	15.3635	14.5680	10.1130	9.2486	−0.5342	10.7670	6.1934
200 ps	16.7426	14.6706	13.4297	11.2098	8.8882	−0.3642	10.7628	6.0937
300 ps	16.3358	14.8949	14.4448	10.8304	8.3576	−0.5524	10.7185	6.2530
400 ps	16.0896	14.8921	12.8989	9.9230	8.4544	−0.5422	10.2860	6.0409
500 ps	15.9855	14.8842	12.1643	10.1569	7.9333	−0.3976	10.1211	5.9445
Average	16.1993	14.9410	13.5011	10.4466	8.5764	−0.4781	10.5311	
S.D.	0.3530	0.2547	1.0227	0.5475	0.5063	0.0898		5.6761

[a] The density of state analysis shows the energy, measured in eV, of the lowest unoccupied molecular orbital as a function of simulation time and solvation. One can observe the trend from the 0 Å water layer to DCPB (continuum) water that the LUMO energies become increasingly stabilized as the system becomes increasingly solvated, while at the same time; the conformational dependence is much less distinct.

Table 9
LUMO energies determined using the PM3 Hamiltonian[a]

	0 Å	2.5 Å	3.5 Å	4.5 Å	5.5A	DCPB	Average	S.D.
100 ps	15.6850	14.9816	14.1374	9.2784	8.2924	−0.5937	10.2968	6.1545
200 ps	16.5020	14.2439	13.1071	10.3171	8.2925	−0.4759	10.3311	6.0340
300 ps	16.1265	14.4898	13.9493	9.9419	7.3798	−0.7355	10.1920	6.2480
400 ps	15.9662	14.5557	12.5124	9.4748	7.9657	−0.6375	9.9729	6.0038
500 ps	15.8039	14.5567	11.7700	9.7007	7.5247	−0.4885	9.8112	5.8923
Average	16.0167	14.5655	13.0952	9.7426	7.8910	−0.5862	10.1208	
S.D.	0.3184	0.2657	0.9889	0.4058	0.4253	0.1080		5.6374

[a] The density of state analysis shows the energy, measured in eV, of the lowest unoccupied molecular orbital as a function of simulation time and solvation. One can observe the trend from the 0 Å water layer to DCPB (continuum) water that the LUMO energies become increasingly stabilized as the system becomes increasingly solvated, while at the same time; the conformational dependence is much less distinct.

and the LUMOs causes the HOMO–LUMO gap to widen upon solvation (see Table 10 for AM1 and Table 11 for PM3).

According to semiconductor theory [80], the magnitude of the band gap is indicative of conductivity where a band gap less then ∼1.5 eV generally indicates that charge can potentially conduct through the gap. DNA in a vacuum shows an average band gap of ∼1 eV clearly indicating that DNA will exhibit semi-conductive properties under these conditions. Upon solvation, the band gap jumps beyond the semiconductor threshold to ∼3 eV for AM1 and ∼2 eV for PM3. Further solvation continues to erode DNA's semi-conductive properties by exhibiting ever-larger band gaps. The results of the continuum simulation yield the largest band gaps observed in this study at 7.7 eV from AM1 and 7.3 eV for PM3.

Both the explicit solvent model and the continuum approach support the claim made in the literature that the band gap appears in those systems incorporating solvent characteristics and diminishes when the system is in a vacuum [53]. Much of the experimental research showing DNA conductivity has been done while the DNA molecule was in a vacuum supporting the proposition that DNA is, indeed, a conducting molecule in vacuo [23,20,21]. Interestingly, at the same time, DNA has also been observed as a conductor in solvent [24–40,22]. Unfortunately, much of the research on solvated systems includes an intercalater that is beyond the scope of this paper [24–40]. Future research could center around the effects of intercalaters on the band gap of DNA biomolecules. Another potentially interesting simulation would be the inclusion of

Table 10
Band gap determined using the AM1 Hamiltonian[a]

	0.0 Å	2.5 Å	3.5 Å	4.5 Å	5.5 Å	PB	Average	S.D.
100 ps	1.0676	2.9113	4.9178	4.0569	5.6424	7.6536	4.3749	2.2730
200 ps	1.9998	3.0802	5.2411	5.4139	5.5859	7.8056	4.8544	2.0496
300 ps	1.0387	3.0354	4.4090	6.2037	7.5104	7.5498	4.9578	2.6132
400 ps	0.7053	3.2135	3.9380	6.4086	6.8134	7.5671	4.7743	2.6200
500 ps	1.1791	2.1565	3.1882	5.3910	6.2971	7.7585	4.3284	2.5576
Average	1.1981	2.8794	4.3388	5.4948	6.3698	7.6669	4.6580	
S.D.	0.4818	0.4183	0.8122	0.9250	0.8134	0.1134		2.2742

[a] The density of state analysis shows the band gap, measured in eV, as a function of simulation time and solvation. One can observe the trend from the 0 Å water layer to DCPB (continuum) water that the gap increase as the system becomes increasingly solvated, while at the same time; the conformational dependence is much less distinct.

Table 11
Band gap determined using the PM3 Hamiltonian[a]

	0.0 Å	2.5 Å	3.5 Å	4.5 Å	5.5 Å	PB	Average	S.D.
100 ps	0.4376	2.3509	4.3397	3.1331	4.7357	7.2647	3.7103	2.3226
200 ps	1.3175	2.5490	4.8467	4.5278	5.0479	7.4295	4.2864	2.1290
300 ps	0.4044	2.5282	3.8888	5.4070	6.5727	7.0940	4.3158	2.5566
400 ps	0.1382	2.8358	3.6020	6.0404	6.3625	7.2115	4.3651	2.6716
500 ps	0.5313	1.7109	2.7454	5.0081	5.9382	7.3594	3.8822	2.6390
Average	0.5658	2.3950	3.8845	4.8233	5.7314	7.2718	4.1120	
S.D.	0.4449	0.4200	0.7922	1.0955	0.8074	0.1302		2.3113

[a] The density of state analysis shows the band gap, measured in eV, as a function of simulation time and solvation. One can observe the trend from the 0 Å water layer to DCPB (continuum) water that the gap increase as the system becomes increasingly solvated, while at the same time; the conformational dependence is much less distinct.

dopants in the solvated DNA. The band gaps we found for solvated DNA are relatively small in magnitude implying that perhaps one could use dopants to affect the band gap.

3.3. Frontier molecular orbital analysis

As noted above, frontier molecular orbital theory stipulates that a reaction is controlled by the interaction and overlap of the frontier orbitals (HOMO and LUMO) and that the reactivity of these orbitals depends upon the energy, symmetry and accessibility of these orbitals [60]. Knowledge of the localization and overall shape of these orbitals will provide insight into the reactivity of the species in question. DNA, being the ''brain'' of the cell, is especially interesting to scientists who want to control the activities of the cell [61,40,66]. For this reason, attention has been paid to the frontier orbital populations of DNA [62].

When the quantum mechanical calculations are complete, one can construct a cube file with the CUBE keyword in DivCon99. With the help of gOpenMol [81], these files lead to the space filling diagrams seen in Figs. 5 and 6. These diagrams illustrate those areas in the biomolecule where the HOMO or LUMO is most localized. In all cases, it appears that these frontier orbitals are localized on a specific base or sets of bases, and they exhibit very little delocalization over the entire molecule. In order to gain a better understanding of which bases the frontier orbitals are most likely to populate one can chart the relative HOMO and LUMO density per orbital per residue. As seen in Fig. 7(a–e) for AM1, the HOMO of each configuration was localized on one residue with very little orbital ''spill over'' into neighboring residues. This is in contrast to Saito et al. [62] where they observed a single residue having the majority of the HOMO and a greater delocalization of the HOMO over two or three residues. Similarly, for Fig. 8(a–e), the HOMOs obtained using PM3 are also mostly localized on a single residue per configuration with one notable exception. The 200 ps snapshot at 5.5 Å solvation shows a delocalization of the HOMO between two neighboring residues. Residue 16 (guanine from Fig. 3b) has ∼53% of the HOMO and residue 17 (adenine from Fig. 3b) has ∼48% of the HOMO.

When comparing the residue numbers in Figs. 7 and 8 with those in Fig. 3b, one will observe that the HOMOs are either mostly localized on the guanine or mostly localized on the adenine depending upon the level of solvation. The literature [62] maintains that in all studied systems, the HOMOs are always localized on a single residue with some HOMO character spilling over to neighboring residues. According to Saito et al. [62], in all cases the HOMO is mostly localized on the Guanine. When cross-referencing Fig. 3b with Figs. 7 and 8, the HOMO is localized either on the adenine (A) or the guanine (G). Experimental results also show that the HOMO is, indeed,

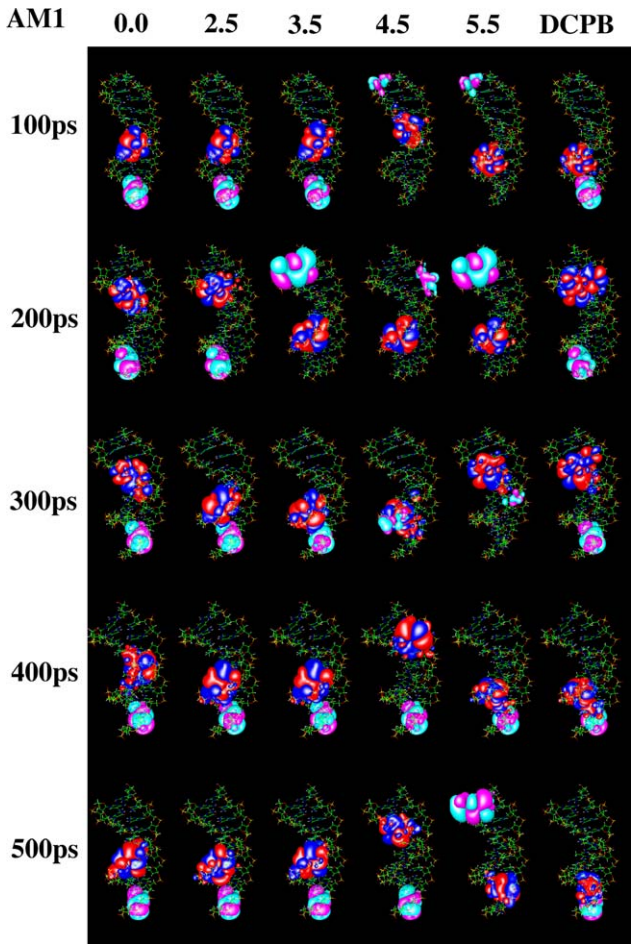

Fig. 5. AM1 space-filling model of the frontier orbitals. In the space-filling model, we can see how the localization of the frontier orbitals change (or remain constant) as a function of both conformation and solvation layer. In these models, the red/blue regions represent the HOMOs and the light-purple/light-blue regions represent the LUMOs.

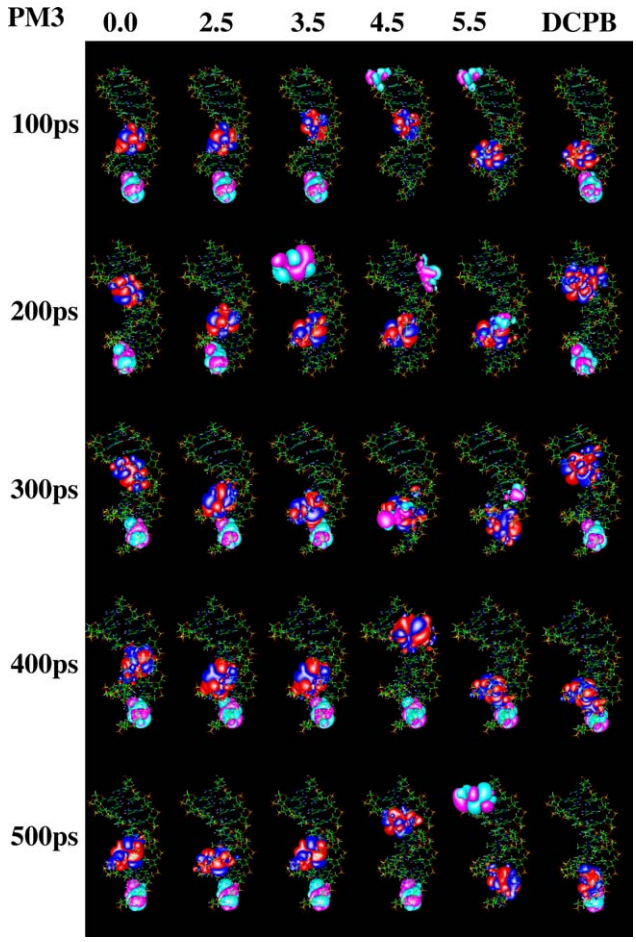

Fig. 6. PM3 space-filling models of frontier orbitals. In the space-filling model, we can see how the localization of the frontier orbitals change (or remain constant) as a function of both conformation and solvation layer. In these models, the red/blue regions represent the HOMOs and the light-purple/light-blue regions represent the LUMOs.

localized on guanine [63,41,62] and theoretical, ab initio research on several in vacuo systems shows that the HOMO is most likely localized on a guanine [62]. These results are in direct contrast to our data where we show that in vacuo systems it is the adenine that will most likely house the HOMO.

The discrepancy between the semi-empirical results described in the present study and the results of the experimental study can be explained when taking into account the solution environment of both studies. As shown in Fig. 7 for AM1 and Fig. 8 for PM3 the HOMO is, indeed, more highly localized on the guanine in the systems with a higher solvation (generally 4.5 Å and 5.5 Å). Since the experimental system presented in Saito et al. [62] are performed while the DNA is immersed in solution, the 4.5 Å and 5.5 Å systems seem to mimic quite well the "infinite" solvation used in the experimental studies. Further, there is a correlation between the energy of the HOMO and the identity of the residue on which the HOMO is localized. As shown in Table 6 for AM1 and Table 7 for PM3, the energy of the HOMO falls as the level of solvation increases. As the energy of the HOMO falls between 4 eV and 5 eV for AM1 and 5 eV and 6 eV for PM3, the HOMO has a greater probability for residing on the guanine while at energies above that band, the HOMO will most likely be found on the adenine. In one instance, the HOMO localization did not follow this trend. For the 200 ps snapshot with a 2.5 Å layer of solvent calculated with the AM1 Hamiltonian, the HOMO does reside on the guanine even though the energy is above the 4–5 eV range. Further research is needed to determine what is unusual about this configuration.

Although this explanation does show a nice correlation that could lead to further research, this explanation does not satisfy the discrepancy between the ab inito data presented in Saito et al. [62] and the semi-empirical data presented in this paper. In order to explain this disparity, one must compare the character of the systems used in both sets of calculations since fundamentally, the systems used in Saito et al. [62] are very different then those used in this paper. When Saito et al. constructed their DNA systems they built their duplexes without ribose and phosphate backbones in order to save some computational expense associated with an ab inito calculation on such a large biomolecule. In place of the normally charged, solvent exposed backbone they employed an uncharged methyl group to fill the open valance. This loss of charge and loss of the interaction energy associated with the phosphate backbone, most likely stabilizes the HOMO enough for it to have a higher probability of being localized on the guanine. This situation could be analogous to when one immerses the DNA in a water bath where the increased solvation leads to greater HOMO stabilization (as observed in the present study). Another factor that differs between the two studies is the use of MD snapshots that are then used in electronic structure calculations. The resultant dynamic effects could alter the localization of the HOMO and LUMOs.

The results obtained from the continuum calculations continued the trend observed in the explicit solvent calculations. In all cases, the HOMO is localized on the guanine instead of the adenine. When one compares the location of the HOMO with the energies found in Table 6 for AM1 and Table 7 for PM3 one will observe that the energy is less than the 4–5 eV-separation band. Further, the continuum calculation mimics a situation of infinite solvation by providing energies lower then those of the 5.5 Å configurations. A much larger solvation layer would need to be used in order to test this hypothesis.

In addition to modeling the HOMOs of each configuration, the LUMOs are also shown in Fig. 9 for AM1 and Fig. 10 for PM3. LUMO localization proved to be much less dynamic then HOMO localization. Generally, the LUMOs were found on the cytosine (residues 1 or 13) at one of the ends of the strand. What is interesting is that unlike the HOMO localization described earlier, the LUMO localization was sometimes found in the surrounding solution instead of on the DNA itself. In Figs. 9 and 10, the residue 25 represents all of the solvent. Fig. 9a (100 ps) and c (300 ps) show that for 5.5 Å, the LUMO has the greatest probability of being found in the water. Similarly, Fig. 10a (100 ps), b (200 ps), and c (300 ps) also yield solvent-bound LUMOs. Obviously, since the continuum configurations include zero water molecules, 100% of the LUMO is localized on the DNA. Based on these 5.5 Å versus continuum results, the explicit solvent configurations may give better density of state results then those provided by the continuum calculations.

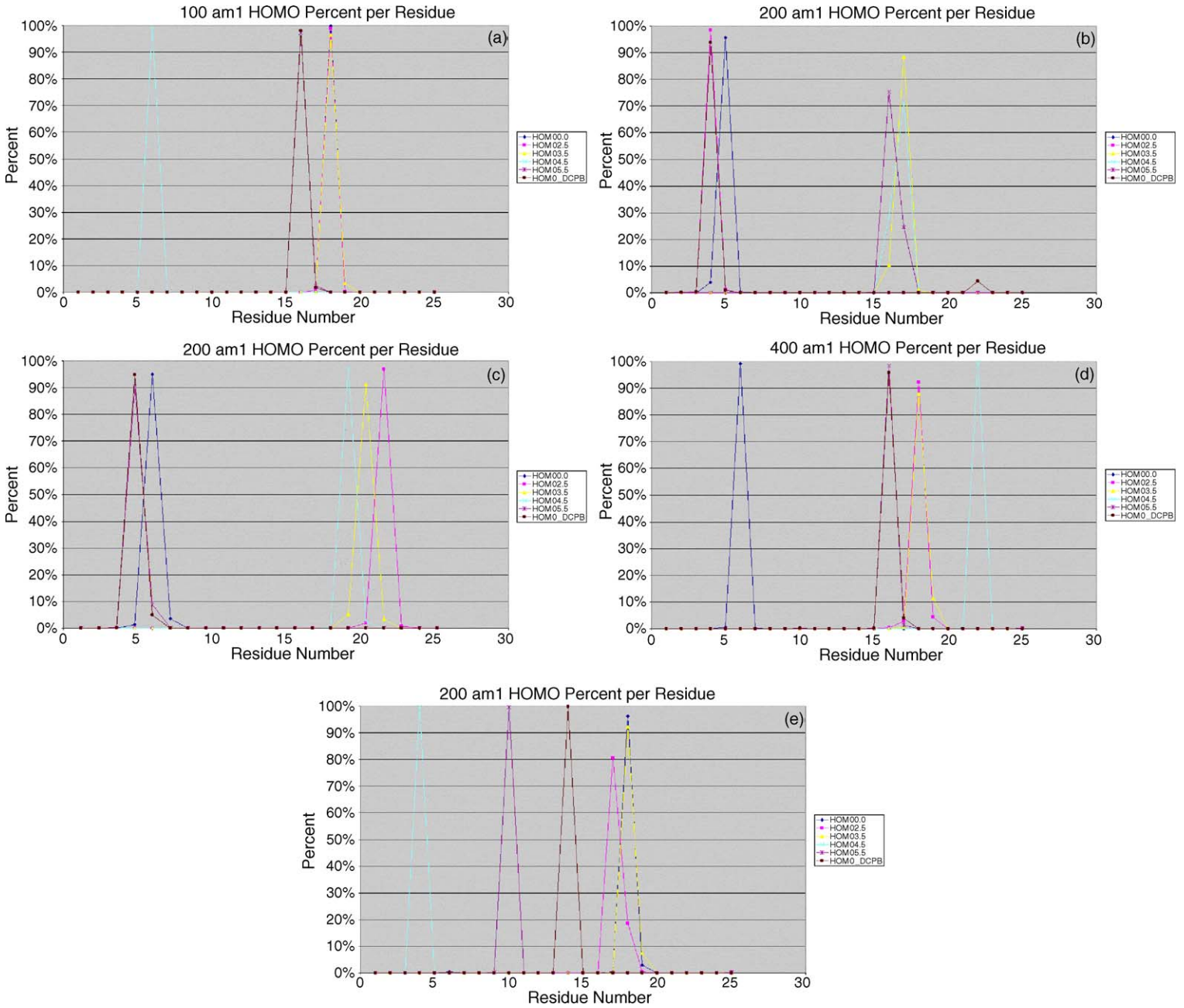

Fig. 7. AM1 HOMO distribution. For a more graphical representation of the HOMO localization, this figure shows the distribution as a function both of conformation and of solvation layer. In each graph, the blue line indicates the DNA in a vacuum, while the pink, yellow, blue, red, and brown lines illustrate the 2.5 Å, 3.5 Å, 4.5 Å, 5.5 Å, and DCPB solvation environments respectively. In each case, the HOMO seems to be localized almost exclusively on a single nucleotide.

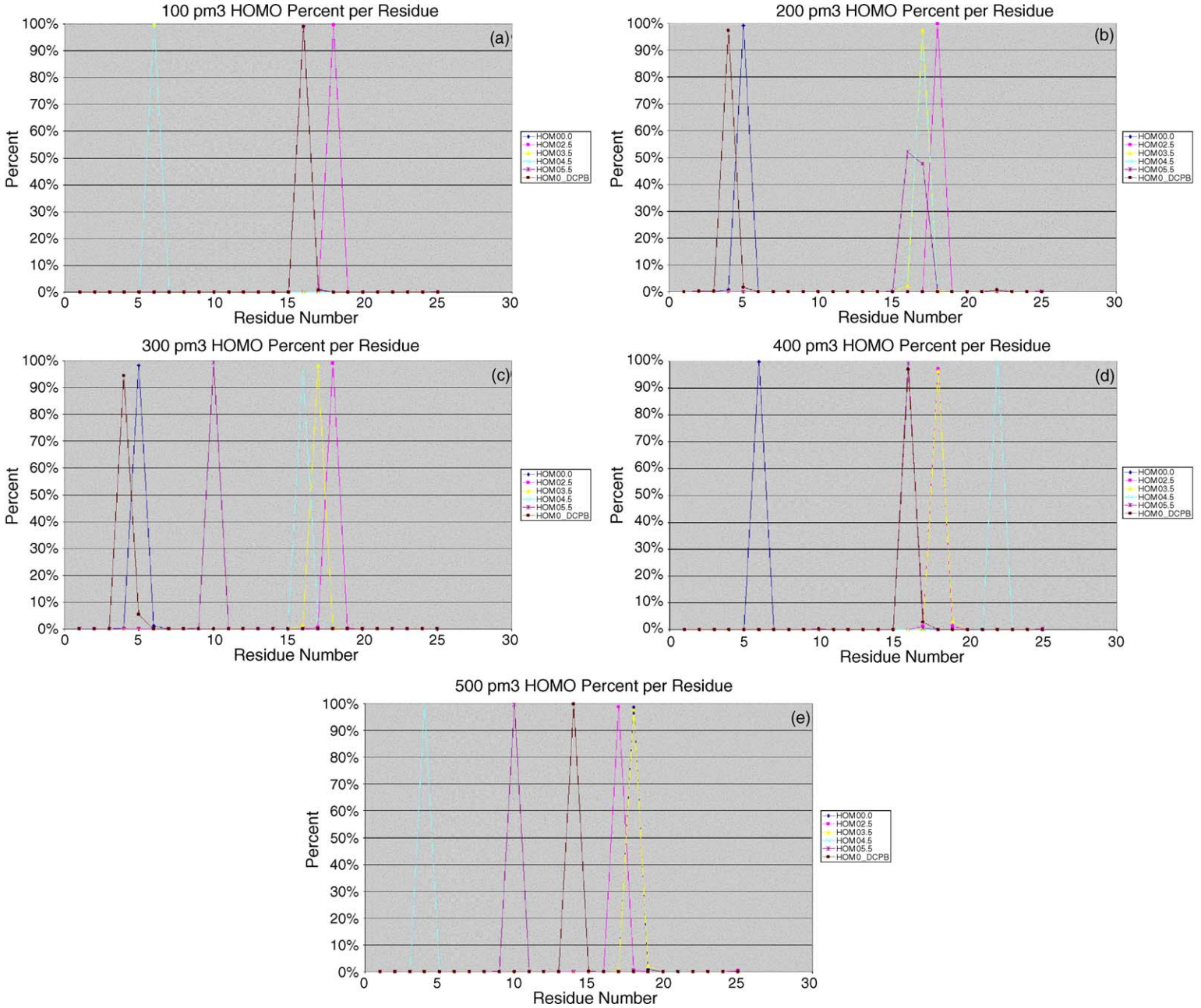

Fig. 8. PM3 HOMO distribution. For a more graphical representation of the HOMO localization, this figure shows the distribution as a function both of conformation and of solvation layer. In each graph, the blue line indicates the DNA in a vacuum, while the pink, yellow, blue, red, and brown lines illustrate the 2.5 Å, 3.5 Å, 4.5 Å, 5.5 Å, and DCPB solvation environments respectively. In almost every case, the HOMO seems to be localized almost exclusively on a single nucleotide. In one instance, the characterization of the 200 ps conformation with the 5.5 Å solvation layer, the HOMO is spread between two nucleotides.

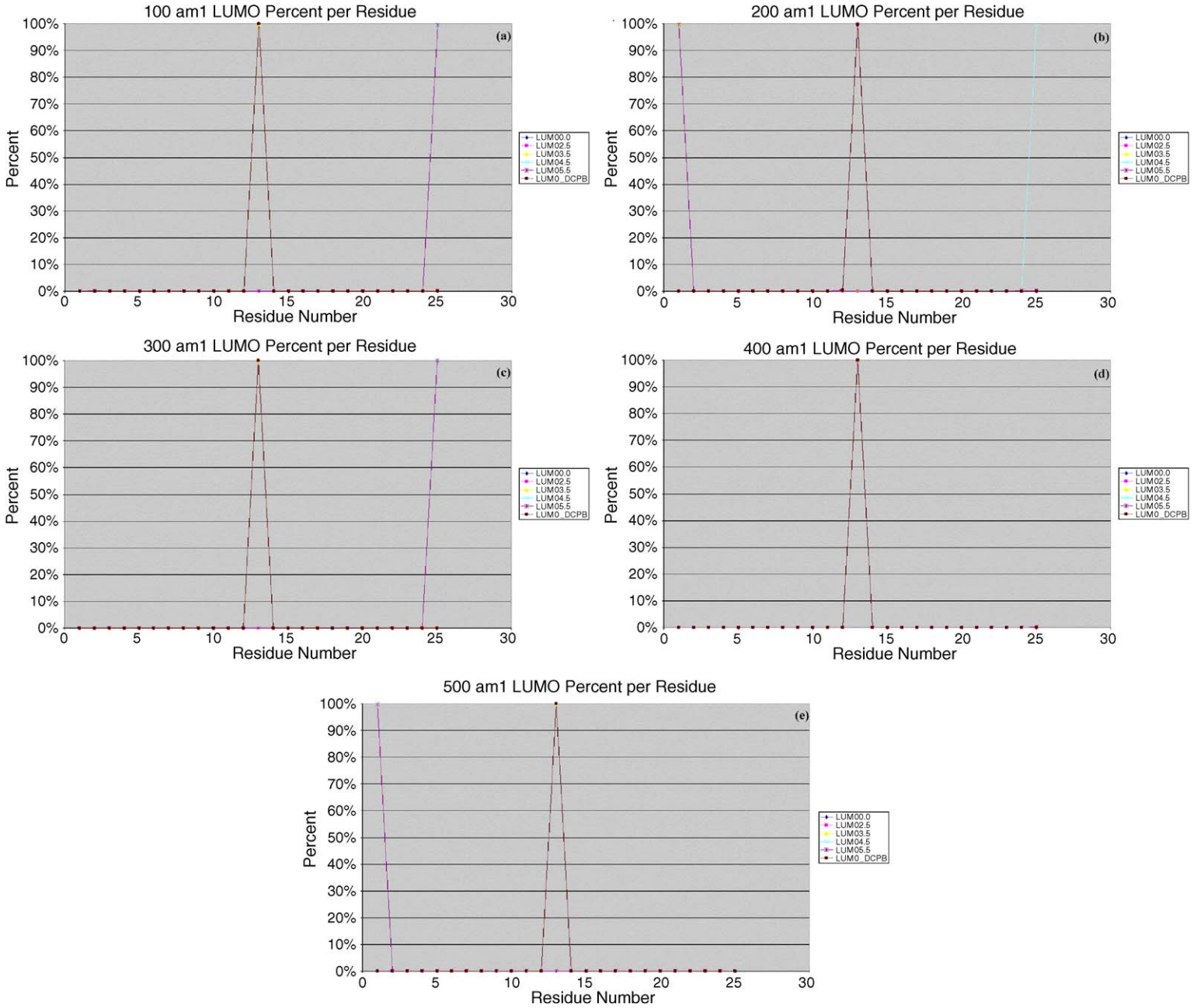

Fig. 9. AM1 LUMO distribution. For a more graphical representation of the LUMO localization, this figure shows the distribution as a function both of conformation and of solvation layer. In each graph, the blue line indicates the DNA in a vacuum, while the pink, yellow, blue, red, and brown lines illustrate the 2.5 Å, 3.5 Å, 4.5 Å, 5.5 Å, and DCPB solvation environments respectively. In every case, the LUMO seems to be localized almost exclusively on a single nucleotide.

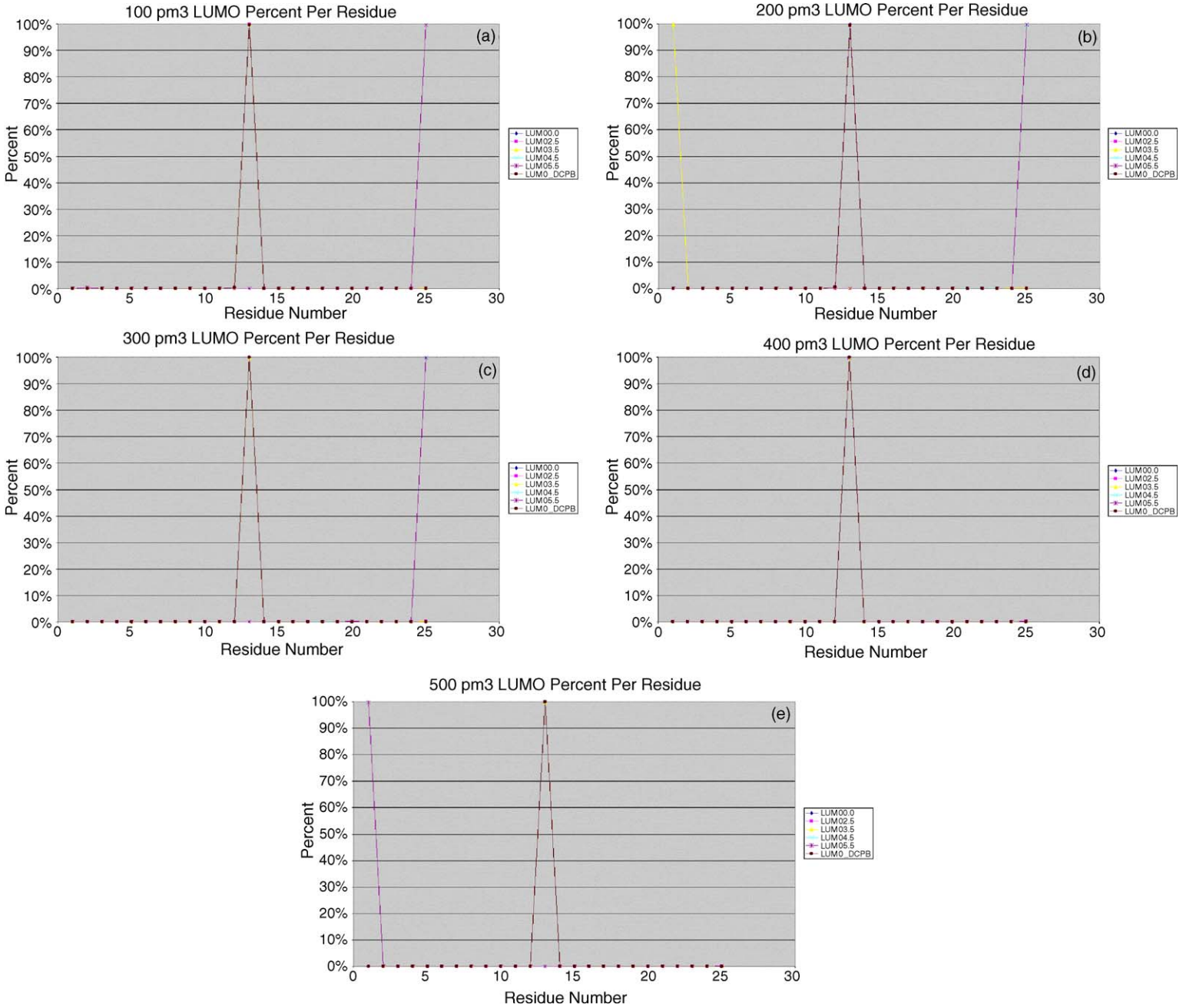

Fig. 10. PM3 LUMO distribution. For a more graphical representation of the LUMO localization, this figure shows the distribution as a function both of conformation and of solvation layer. In each graph, the blue line indicates the DNA in a vacuum, while the pink, yellow, blue, red, and brown lines illustrate the 2.5 Å, 3.5 Å, 4.5 Å, 5.5 Å, and DCPB solvation environments respectively. In every case, the LUMO seems to be localized almost exclusively on a single nucleotide.

11.0 Å solvation configurations would be important to determine whether or not these solvent-bound LUMOs are simply artifacts of these particular configurations, or if this is a characteristic of highly solvated DNA systems.

4. Conclusions

Through molecular dynamics, quantum mechanics, and visualization various electrical properties of DNA have been successfully studied. The energy levels of both the HOMO and the LUMO of DNA are affected by greater solvation showing that the electronic properties of DNA are greatly affected by solvation. For instance, when the DNA is placed in a vacuum it shares characteristics with semiconductors that support the position of others that DNA is, in deed, a conductor in certain environments. Further, since even at its largest the band gap is still relatively small compared to most insulators (see Tables 10 and 11), it may be possible to ''dope'' the DNA to improve conductivity in solution. Unfortunately, also due to limitations in the methods, a definitive answer as to the nature of the mechanism long range charge transfer cannot be made. One possibility would be that while in vacuo the DNA acts as a semiconductor, while in solution the DNA transfers electrons via a different mechanism.

This study provided a great opportunity to compare both the explicit solvent and the implicit (continuum) solvent methods. The continuum method seems to do relatively well mimicking conditions of infinite solvation in the sense that the results it generates follow the trends established by the explicitly solvated systems. Where the method may breakdown is in the treatment of the LUMO. In this case, though the energy calculated seems to follow the LUMO energy trend generated by the explicit solvent treatment, the localization is different. Conversely, the determination of the HOMO localization seems to be similar to that observed in the 5.5 Å explicit solvent configurations. Therefore, it is apparent that while the continuum method may not perfectly describe the system in all cases, in most situations, the method does reasonably well.

Acknowledgments

We would like to thank the DOE (DE-FGO2-96ER62270) for supporting this research. We also thank the Pittsburgh Supercomputer Center, the San Diego Supercomputer Center and the National Center for Supercomputer Applications for generous allocations of supercomputer time.

References

[1] P.J. Dandliker, R.E. Holmlin, J.K. Barton, Oxidative thymine dimer repair in the DNA helix, Science 275 (1997) 1465–1468.
[2] D. Voet, J.G. Voet, Biochemistry, John Wiley & Sons, Inc., New York, 1995
[3] T.E. Creighton, Proteins, Structures and Molecular Properties, W. H. Freeman, New York, 1993.
[4] G.A. Jeffrey, W. Sarnger, Hydrogen Bonding in Biological Structures, Springer-Verlag, Heidelberg, 1991.
[5] A. van der Vaart, K.M. Merz Jr., Divide and conquer interaction energy decomposition, J. Phys. Chem. A 103 (1999) 3321–3329.
[6] A. van der Vaart, K.M. Merz Jr., The role of polarization and charge transfer in the solvation of biomolecules, J. Am. Chem. Soc. 121 (1999) 9182–9190.
[7] C.L. Brooks III, D.A. Case, Chem. Rev. 93 (1993) 2487–2502.
[8] B.M. Pettit, J.C. Smith, Comput. Phys. Commun. 91 (1995) 1–344.
[9] J. Gao, X. Xia, Science 258 (1992) 631–635.
[10] H. Lodish, D. Baltimore, A. Berk, S.L. Zipursky, P. Matsudaira, J. Darnell, Molecular Cell Biology, Scientific American Books, New York, 1995.
[11] S. Steenken, Purine bases, nucleosides, and nucleotides: aqueous solution redox chemistry and transformation reactions of their radical cations and e^- and OH adducts, Chem. Rev. 89 (1989) 503– ‘520.
[12] B. Armitage, Photocleavage of nucleic acids, Chem. Rev. 98 (1998) 1171–1200.
[13] C.J. Burrows, J.G. Muller, Oxidative nucleobase modifications leading to strand scission, Chem. Rev. 98 (1998) 1109–1151.
[14] H.-C. Lee, M.L.R. Lim, C.-Y. Lu, V.W.S. Liu, H.-J. Fahn, C. Zhang, P. Nagley, Y.-H. Wei, Concurrent increase of oxidative DNA damage and lipid peroxidation together with mitochondrial DNA mutation in lung tissues during aging—smoking enhances oxidative stress on the aged tissue, Arch. Biochem. Biophys. 362 (2) (1999) 309–316.
[15] S. Kawanishi, S. Oikawa, M. Murata, H. Tsukitome, I. Saito, Site-specific oxidation at GG and GGG sequences in double-stranded DNA by benzoyl peroxide as a tumor promoter, Biochemistry 38 (1999) 16733–16739.
[16] Y. Yoshinoka, Y. Kitagawa, Y. Takano, K. Yamaguchi, T. Nakamura, I. Saito, Experimental and theoretical studies on the selectivity of GGG triplets toward one-electron oxidation in B-form DNA, J. Am. Chem. Soc. 121 (1999) 8712–8719.
[17] P.F. Heelis, S. Liu, Photoenzymic repair of the DNA 6-4 photoproduct—a density functional theory and semiempirical study, J. Am. Chem. Soc. 119 (1997) 2936–2937.
[18] G. Taubes, Double helix does chemistry at a distance—but how? Science 275 (1997) 1420–1421.
[19] D. Porath, A. Bezryadin, S. de Vries, C. Dekker, Direct measurement of electrical transport through DNA molecules, Nature 403 (2000) 635–638.
[20] H.-W. Fink, C. Schonenberger, Electrical conduction through DNA molecules, Nature 398 (1999) 407–410.
[21] G. Hartwich, D.J. Caruana, T. de Lumley-Woodyear, Y. Wu, Electrochemical study of electron transport through thin DNA films, J. Am. Chem. Soc. 121 (1999) 10803–10812.
[22] A. Messer, K. Carpenter, K. Forzley, J. Buchanan, S. Yang, Y. Razskazovskii, Z. Cai, M.D. Sevilla, Electron spin resonance study of electron transfer rates in DNA: determination of the tunneling constant ß for single-step excess electron transfer, J. Phys. Chem. B 104 (2000) 1128–1136.
[23] M.G. Debije, M.T. Milano, W.A. Bernhard, DNA responds to ionizing radiation as an insulator, not as a ''molecular wire'', Angew. Chem. Int. Ed. 38 (18) (1999) 2752–2756.
[24] J.K. Barton, C.V. Kumar, N.J. Turro, DNA-mediated photoelectron transfer reactions, J. Am. Chem. Soc. 108 (1986) 6391–6393.
[25] P. Fromherz, B. Rieger, Photoinduced electron transfer in DNA matrix from intercalated ethidium to condensed methylviologen, J. Am. Chem. Soc. 108 (1986) 5361–5362.
[26] M.D. Purugganan, C.V. Kumar, N.J. Turro, J.K. Barton, Accelerated electron transfer between metal complexes mediated by DNA, Science 241 (1988) 1645–1649.
[27] P.M. Cullis, J.D. McClymont, M.C.R. Symons, Electron conduction and trapping in DNA: an electron spin resonance study, J. Chem. Soc., Faraday Trans. 86 (3) (1990) 591–592.
[28] R.F. Anderson, K.B. Patel, W.R. Wilson, Pulse radiolysis studies of electron migration in DNA from DNA base-radical anions to nitroacridine intercalators in aqueous solution, J. Chem. Soc., Faraday Trans. 87 (23) (1991) 3739–3746.
[29] A.M. Brun, A. Harriman, Dynamics of electron transfer between intercalated polycyclic molecules: effect of interspersed bases, J. Am. Chem. Soc. 114 (1992) 3656–3660.
[30] C.J. Murphy, M.R. Arkin, Y. Jenkins, N.D. Ghatlia, S.H. Bossmann, N.J. Turro, J.K. Barton, Long-range photoinduced electron transfer through a DNA helix, Science 262 (1993) 1025–1029.

[31] A.M. Brun, A. Harriman, Energy- and electron-transfer processes involving palladium porphyrins bound to DNA, J. Am. Chem. Soc. 116 (1994) 10383–10393.
[32] T.J. Meade, J.F. Kayyem, Electron transfer through DNA: site-specific modification of duplex DNA with ruthenium donors and acceptors, Angew. Chem. Int. Ed. 34 (3) (1995) 352–354.
[33] M.R. Arkin, E.D.A. Stemp, R.E. Holmlin, J.K. Barton, A. Hormann, E.J.C. Olson, P.F. Barbara, Rates of DNA-mediated electron transfer between metallointercalators, Science 273 (1996) 475–480.
[34] M.R. Arkin, E.D.A. Stemp, C. Turro, N.J. Turro, J.K. Barton, Luminescence quenching in supramolecular systems: a comparison of DNA- and SDS micelle-mediated photoinduced electron transfer between metal complexes, J. Am. Chem. Soc. 118 (1996) 2267–2274.
[35] D.B. Hall, R.E. Holmlin, J.K. Barton, Oxidative DNA damage through long-range electron transfer, Nature 382 (1996) 731–735.
[36] R.E. Holmlin, E.D.A. Stemp, J.K. Barton, $Os(phen)_2dppz^{2+}$ in photoinduced DNA-mediated electron transfer reactions, J. Am. Chem. Soc. 118 (1996) 5236–5244.
[37] A. Pezeshk, M.C.R. Symons, J.D. McClymont, Electron movement along DNA strands: use of intercalators and electron paramagnetic resonance spectroscopy, J. Chem. Phys. 100 (1996) 18562–18566.
[38] S.M. Gasper, G.B. Schuster, Intramolecular photoinduced electron transfer to anthraquinones linked to duplex DNA: the effect of gaps and traps on long-range radical cation migration, J. Am. Chem. Soc. 119 (1997) 12762–12771.
[39] D. Ly, L. Sanii, G.B. Schuster, Mechanism of charge transport in DNA: internally-linked anthraquinone conjugates support phonon-assisted polaron hopping, J. Am. Chem. Soc. 121 (1999) 9400–9410.
[40] S.R. Rajski, S. Kumar, R.J. Roberts, J.K. Barton, Protein-modulated DNA electron transfer, J. Am. Chem. Soc. 121 (1999) 5615–5616.
[41] I. Saito, T. Nakamura, K. Nakatani, Y. Yoshioka, K. Yamaguchi, H. Sugiyama, Mapping of the hot spots for DNA damage by one-electron oxidation: efficacy of GG doublets and GGG triplets as a trap in long-range hole migration, J. Am. Chem. Soc. 120 (1998) 12686–12687.
[42] B. Giese, S. Wessely, M. Spormann, U. Lindemann, E. Meggers, M.E. Michel-Beyerle, On the mechanism of long-range electron transfer through DNA, Angew. Chem. Int. Ed. 38 (7) (1999) 996–998.
[43] P.T. Henderson, D. Jones, G. Hampikian, Y. Kan, G.B. Schuster, Long-distance charge transport in duplex DNA: the phonon-assisted polaron-like hopping mechanism, Proc. Natl. Acad. Sci. U.S.A. 96 (1999) 8353–8358.
[44] B. Giese, long-distance charge transport in DNA: the hopping mechanism, Acc. Chem. Res. 33 (2000) 631–636.
[45] E.J.C. Olson, D. Hu, A. Hormann, P.F. Barbara, Quantitative modeling of DNA-mediated electron transfer between metallointercalators, J. Phys. Chem. B 101 (1997) 299–303.
[46] J. Jortner, M. Bixon, T. Langenbacher, M.E. Michel-Beyerle, Charge transfer and transport in DNA, Proc. Natl. Acad. Sci. U.S.A. 95 (1998) 12759–12765.
[47] F.C. Grozema, Y.A. Berlin, L.D.A. Siebbeles, Sequence-dependent charge transfer in donor–DNA–acceptor systems: a theoretical study, Int. J. Quantum Chem. 75 (1999) 1009–1016.
[48] Y.A. Berlin, A.L. Burin, M.A. Ratner, On the long-range charge transfer in DNA, J. Phys. Chem. 104 (3) (2000) 443–445.
[49] M.D. Sevilla, B. Besler, A.-O. Colson, Ab initio molecular orbital calculations of DNA radical ions. 5. Scaling of calculated electron affinities and ionization potentials to experimental values, J. Phys. Chem. 99 (1995) 1060–1063.
[50] J. Sponer, J. Leszczynski, P. Hobza, Nature of nucleic acid–base stacking: nonempirical ab initio and empirical potential characterization of 10 stacked base dimers. Comparison of stacked and H-bonded base pairs, J. Phys. Chem. B 100 (1996) 5590–5596.
[51] H. Sugiyama, I. Saito, Theoretical studies of GG-specific photocleavage of DNA via electron transfer: significant lowering of ionization potential and 5′-localization of HOMO of stacked GG bases in B-form DNA, J. Am. Chem. Soc. 118 (1996) 7063–7068.
[52] F. Prat, K.N. Houk, C.S. Foote, Effect of guanine stacking on the oxidation of 8-oxoguanine in B-DNA, J. Am. Chem. Soc. 120 (1998) 845–846.
[53] D.M. York, T.-S. Lee, W. Yang, Quantum mechanical treatment of biological macromolecules in solution using linear-scaling electronic structure methods, Phys. Rev. Lett. 80 (1998) 5011–5014.
[54] G. Nadig, L.C. Van Zant, S.L. Dixon, K.M. Merz Jr., Charge-transfer interactions in macromolecular systems: a new view of the protein/water interface, J. Am. Chem. Soc. 120 (1998) 5593–5594.
[55] W. Yang, T.-S. Lee, A density-matrix form of the divide-and-conquer approach for electronic structure calculations of large molecules, J. Chem. Phys. 103 (13) (1995) 5674–5678.
[56] S.L. Dixon, K.M. Merz Jr., Semiempirical molecular orbital calculations with linear system size scaling, J. Chem. Phys. 104 (1996) 6643–6649.
[57] S.L. Dixon, K.M. Merz Jr., Fast, accurate semiempirical molecular orbital calculations for macromolecules, J. Chem. Phys. 107 (3) (1997) 879–893.
[58] V. Gogonea, K.M. Merz Jr., Fully quantum mechanical description of proteins in solution. Combining linear scaling quantum mechanical methodologies with the Poisson–Boltzman equation, J. Phys. Chem. A 103 (26) (1999) 5171–5188.
[59] K. Fukui, Recognition of stereochemical paths by orbital interaction, Acc. Chem. Res. 4 (1971) 57–64.
[60] I. Fleming, Frontier orbitals and organic chemical reactions, John Wiley & Sons, 1976.
[61] H. Kagawa, K. Mori, Molecular orbital study of the interaction between MgATP and the myosin motor domain: the highest occupied molecular orbitals indicate the reaction site of ATP hydrolysis, J. Phys. Chem. B 103 (1999) 7346–7352.
[62] I. Saito, T. Nakamura, N. Kazuhiko, Mapping of highest occupied molecular orbitals of duplex DNA by cobalt-mediated guanine oxidation, J. Am. Chem. Soc. 122 (2000) 3001–3006.
[63] I. Saito, M. Takayama, H. Sugiyama, K. Nakatani, Photoinduced DNA cleavage via electron transfer: demonstration that guanine residues located 5′ to guanine are the most electron-donating sites, J. Am. Chem. Soc. 117 (1995) 6406–6407.
[64] A. van der Vaart, B.D. Bursulaya, C.L. Brooks III, K.M. Merz Jr., Are many-body effects important in protein folding? J. Phys. Chem. B 104 (2000) 9554–9563.
[65] A. van der Vaart, K.M. Merz Jr., Charge transfer in biologically important molecules: a comparison of high level ab initio and semiempirical methods, Int. J. Quantum Chem. 77 (2000) 27–43.
[66] H.-A. Wagenknecht, E.D.A. Stemp, J.K. Barton, Evidence of electron transfer from peptides to DNA: oxidation of DNA-bound tryptophan using the flash-quench technique, J. Am. Chem. Soc. 122 (1) (2000) 1–7.
[67] H.R. Drew, R.M. Wing, T. Takano, C. Broka, S. Tanaka, K. Itakura, R.E. Dickerson, Structure of a B-DNA Dodecamer. Conformation and Dynamics, Proc. Natl. Acad. Sci. U.S.A. 78 (1981) 2179.
[68] W.L. Jorgensen, J. Chandrasekhar, J. Madura, R.W. Impey, M.L. Klein, Comparison of simple potential functions for the simulation of liquid water, J. Chem. Phys. 79 (1983) 926.
[69] D.A. Case, D.A. Pearlman, J.W. Caldwell, T.E. Cheatham III, W.S. Ross, C.L. Simmerling, T.A. Darden, K.M. Merz Jr., R.V. Stanton, A.L. Cheng, J.J. Vincent, M. Crowley, D.M. Ferguson, R.J. Radmer, G.L. Seibel, U.C. Singh, P.K. Weiner, P.A. Kollman, AMBER, University of California, San Francisco, 1997.
[70] P. Auffinger, E. Westhof, Simulations of the molecular dynamics of nucleic acids, Curr. Op. Struct. Biol. 8 (1998) 227–236.
[71] A. Cheng, R.S. Stanton, J.J. Vincent, K.V. Damodaran, S.L. Dixon, D.S. Hartsough, S.A. Best, K.M.J. Merz, ROAR, The Pennsylvania State University, University Park, PA, 1997.
[72] W.D. Cornell, P. Cieplak, C.I. Bayly, I.R. Gould, K.M. Merz Jr., D.M. Ferguson, D.C. Spellmeyer, T. Fox, J.W. Caldwell, P.A. Kollman, A second generation force field for the simulation of proteins, nucleic acids, and organic molecules, J. Am. Chem. Soc. 117 (19) (1995) 5179–5197.
[73] H.J.C. Berendsen, J.P.M. Potsma, W.F. van Gunsteren, A.D. DiNola, J.R. Haak, Molecular dynamics with coupling to an external bath, J. Chem. Phys. 81 (1984) 3684–3690.

[74] M.P. Allen, D.J. Tildesley, Computer Simulation of Liquids, Clarendon Press, Oxford, 1987.
[75] M.J.S. Dewar, E.G. Zoebisch, E.F. Healy, J.J.P. Stewart, AM1: a new general purpose quantum mechanical molecular model, J. Am. Chem. Soc. 107 (13) (1985) 3902–3909.
[76] J.J.P. Stewart, Optimization of parameters for semiempirical methods I. Method, J. Comp. Chem. 10 (2) (1989) 209–220.
[77] J.J.P. Stewart, Optimization of parameters for semiempirical methods II. Applications, J. Comp. Chem. 10 (2) (1989) 221–264.
[78] S.L. Dixon, A. van der Vaart, V. Gogonea, J.J. Vincent, E.N. Brothers, L.M. Westerhoff, K.M.J. Merz, DivCon99, The Pennsylvania State University, University Park, PA, 1999.
[79] E.N. Brothers, K.M. Merz Jr., Sodium parameters for AM1/PM3 optimized using a modified genetic algorithm, J. Chem. Phys. 106 (2002) 2779–2785.
[80] D.C. Giancoli, Physics, Prentice Hall, Englewood Cliffs, New Jersey, 1995
[81] L. Laaksonen, gOpenMol, Espoo, Finland, Center for Scientific Computing, 1999.